J. Fluid Mech. (2004), *vol.* 501, *pp.* 279–301.
DOI: 10.1017/S0022112003007213 Printed in the United Kingdom

The motion of a viscous drop through a cylindrical tube

By S. R. HODGES[1], O. E. JENSEN[2] AND J. M. RALLISON[1]

[1]Department of Applied Mathematics and Theoretical Physics, Centre for Mathematical Sciences, University of Cambridge, Wilberforce Road, Cambridge CB3 0WA, UK

[2]School of Mathematical Sciences, University of Nottingham, University Park, Nottingham NG7 2RD, UK

(Received 27 January 2003 and in revised form 22 September 2003)

Liquid of viscosity μ moves slowly through a cylindrical tube of radius R under the action of a pressure gradient. An immiscible force-free drop having viscosity $\lambda\mu$ almost fills the tube; surface tension between the liquids is γ. The drop moves relative to the tube walls with steady velocity U, so that both the capillary number $Ca = \mu U/\gamma$ and the Reynolds number are small. A thin film of uniform thickness ϵR is formed between the drop and the wall. It is shown that Bretherton's (1961) scaling $\epsilon \propto Ca^{2/3}$ is appropriate for all values of λ, but with a coefficient of order unity that depends weakly on both λ and Ca. The coefficient is determined using lubrication theory for the thin film coupled to a novel two-dimensional boundary-integral representation of the internal flow. It is found that as λ increases from zero, the film thickness increases by a factor $4^{2/3}$ to a plateau value when $Ca^{-1/3} \ll \lambda \ll Ca^{-2/3}$ and then falls by a factor $2^{2/3}$ as $\lambda \to \infty$. The multi-region asymptotic structure of the flow is also discussed.

1. Introduction

We investigate the effect of viscosity on the motion of a drop through a cylindrical tube. The tube has radius R and contains fluid of viscosity μ. An axisymmetric drop of a second immiscible fluid of viscosity $\lambda\mu$ and volume larger than $4\pi R^3/3$ is driven slowly through the tube by a pressure gradient, so that it moves relative to the tube walls with a steady velocity U, as sketched in figure 1. Surface tension γ between the two fluids is taken to be uniform, and both gravity and inertia are assumed negligible. We suppose that the displaced fluid wets the tube wall so that a thin film is established between the drop and the tube, having uniform thickness ϵR away from the front of the drop, where $\epsilon \ll 1$. The problem is controlled by two independent parameters: the viscosity ratio λ; and the capillary number $Ca = \mu U/\gamma$. Our aim is to predict the thickness ϵ as a function of λ and Ca in the limit $Ca \ll 1$.

Bretherton (1961) considered this problem in the case $\lambda = 0$, when the drop is an inviscid bubble. The shape of a semi-infinite bubble in the low-Ca limit consists of a hemispherical cap (region II_o in figure 1) connected to an annular film (region I_o) where the bubble has radius $R(1-\epsilon)$. In the short intervening transition region (region III_o) there is a rapid curvature change and surface tension induces a pressure gradient that drives a flow from region I_o to region II_o. Bretherton showed that the film thickness ϵ is proportional to $Ca^{2/3}$ when $Ca \ll 1$ and is determined in region III_o alone, whose length scales as $Ca^{1/3}R$. A sketch of this argument is provided in

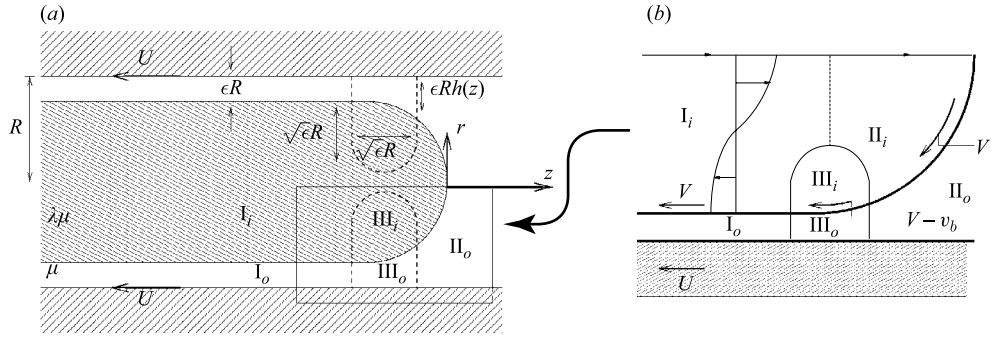

FIGURE 1. Sketch of a semi-infinite drop moving steadily through a cylindrical tube in the frame of the drop tip, showing distinct asymptotic regions. The subscripts '*o*' and '*i*' denote regions outside and inside the drop, respectively. The boundary between regions I_i (the cylindrical body of the drop) and II_i (the cap) is artificial; velocity and lengthscales are the same in both. The magnitude of the internal fluid velocity is V in I_i and II_i and $V - v_b$ in III_i.

§ 2.1 below. The overall bubble length is irrelevant to this result provided that it is sufficiently large for the transition regions at the front and rear of the bubble to be well separated (see, for example, the computations of Martinez & Udell 1990).

Park & Homsy (1984) considered a drop of viscous fluid ($\lambda > 0$) in a Hele-Shaw cell in the limit $Ca \ll 1$. They noted that Bretherton's prediction for the film thickness is unaffected provided $\lambda \ll Ca^{-1/3}$, because only for very viscous drops are the dynamics of the transition region modified. Even so, for $1 \lesssim \lambda \ll Ca^{-1/3}$ the internal and external flows interact (albeit passively) around the cap of the drop. Once $\lambda = O(Ca^{-1/3})$, however, there is a non-trivial coupling between the internal and external flows in region III, extending a distance $Ca^{1/3}R \sim \epsilon^{1/2}R$ into the drop (figure 1). Fortunately, since region III_o has small aspect ratio and region III is small compared to the tube radius, the Stokes flow in region III_i reduces to that in a two-dimensional half-space. We will investigate this interaction below by coupling lubrication theory for region III_o to a boundary-integral description of the flow in region III_i.

For more viscous drops ($Ca^{-1/3} \ll \lambda$) it turns out that the internal and external flows in region III decouple once again. The boundary velocity in the transition region is now the sum of two parts: a slowly varying velocity corresponding to the global flow within the drop; and an additional part that varies on the much shorter lengthscale of the transition region itself. Provided the boundary velocity in the transition region can be found, the film thickness can be determined. We will show, for example, that once λ is increased to the range $Ca^{-1/3} \ll \lambda \ll Ca^{-2/3}$, stresses associated with the recirculating flow within the drop on the lengthscale R generate a velocity on the interface that matches that of the wall. As is well known from studies of surfactant-laden drops in tubes (e.g. Ratulowski & Chang 1990), such an interfacial flow leaves the scaling $\epsilon \sim Ca^{2/3}$ unaltered but increases the film thickness by a factor of $4^{2/3}$ relative to the $\lambda = 0$ case. When λ becomes as large as $Ca^{-2/3}$, however, a further modification takes place. Again the scaling $\epsilon \sim Ca^{2/3}$ is valid, but the sluggish internal flow reduces the interfacial velocity in the transition region, leading to a reduction in film thickness. As $\lambda \to \infty$, the drop boundary becomes effectively rigid everywhere (a limit treated by Bretheron 1961) and the film thickness ends up only a factor of $2^{2/3}$ thicker than the $\lambda = 0$ case.

We therefore predict that the largest film thickness occurs for intermediate values of λ, when $Ca^{-1/3} \ll \lambda \ll Ca^{-2/3}$. Our conclusion differs from that of Schwartz, Princen

& Kiss (1986), who overlooked the intermediate-λ regime. Our prediction appears to be new for this problem, although thickening of films by a factor $4^{2/3}$ has been recognized previously for other coating systems (e.g. Shen *et al.* 2002). In particular, the thickening factor $4^{2/3}$ found by Ratulowski & Chang (1990), Stebe, Lin & Maldarelli (1991) and Park (1991) for surfactant-laden bubbles moving through tubes agrees with experimental results for some surfactant systems (Carroll & Lucassen 1973) although, as noted by Quéré (1999), observations usually show a smaller factor (see also Quéré De Ryck & Ou Ramdane 1997; Ou Ramdane & Quéré 1997). Similarly, we do not expect the plateau in film thickness in the present surfactant-free problem to be observed easily in experiment: for $Ca^{-1/3}$ and $Ca^{-2/3}$ to be separated by at least an order of magnitude requires $Ca \ll 10^{-3}$, for example. Nevertheless detailed estimates below indicate that thickening of around 10% may arise for $30 < \lambda < 100$ when $Ca = 10^{-3}$. We are not aware of any experimental or numerical observations of such thickening for non-surfactant systems. Despite the potential experimental difficulties, we believe that the insights offered by our analysis will be useful in understanding the physical mechanisms operating in this system, and that the methods and results described here may apply also to calculations of film thickness for coating and meniscus-forming flows (see Quéré 1999) where a second viscous fluid is present.

The scalings and governing equations for the problem are described in § 2 and § 3. We show in particular that, when $1 \ll \lambda \ll Ca^{-1/3}$ and $Ca^{-1/3} \ll \lambda \ll Ca^{-2/3}$, the transitional zone between regions I and II develops a nested structure, with new (but passive) regions encircling region III (see Appendices A and B). In order to compute the coupled internal and external flows in region III when $\lambda = O(Ca^{-1/3})$, we present a novel variant on the boundary-integral technique for Stokes flows in Appendix C. Numerical results are given in § 4 and are discussed in § 5.

2. Scaling estimates

We begin by using scaling arguments to develop an overall physical picture of the flow. It is convenient to treat $\epsilon \ll 1$ and λ as independent parameters and then to determine the corresponding value of $Ca \ll 1$. Detailed analysis supporting the scaling arguments is presented in §§ 3 and 4.

2.1. *Drop description and lengthscales*

We suppose that the drop has the steady shape illustrated in figure 1. The film has uniform thickness ϵR away from the front of the drop.

With cylindrical polar coordinates (Rr, Rz) fixed relative to the leading edge of the drop, the tube is at $r = 1$ and the drop boundary is $r(z) = 1 - \epsilon h(z)$ in $z \leqslant 0$, where $h(z)$ is the non-dimensional film thickness. The curvature κ/R of the interface is therefore

$$\kappa = \frac{1}{r\left(1 + r_z^2\right)^{1/2}} - \frac{r_{zz}}{\left(1 + r_z^2\right)^{3/2}}, \tag{2.1}$$

which varies over region III from approximately $2/R$ in the hemispherical cap to $1/R$ in the cylindrical region I. Since $r_{zz} = -\epsilon h_{zz}$, region III has length scaling as $\epsilon^{1/2}R$. Surface tension gives rise to an axial pressure gradient in the film of magnitude $\gamma/(\epsilon^{1/2}R^2)$. Assuming, as we check below, that viscous stress gradients in the drop are no larger than this estimate, a steady lubricating flow is driven in the film with velocity scaling as $\gamma\epsilon^{3/2}/\mu$. This velocity must be comparable to the speed of the

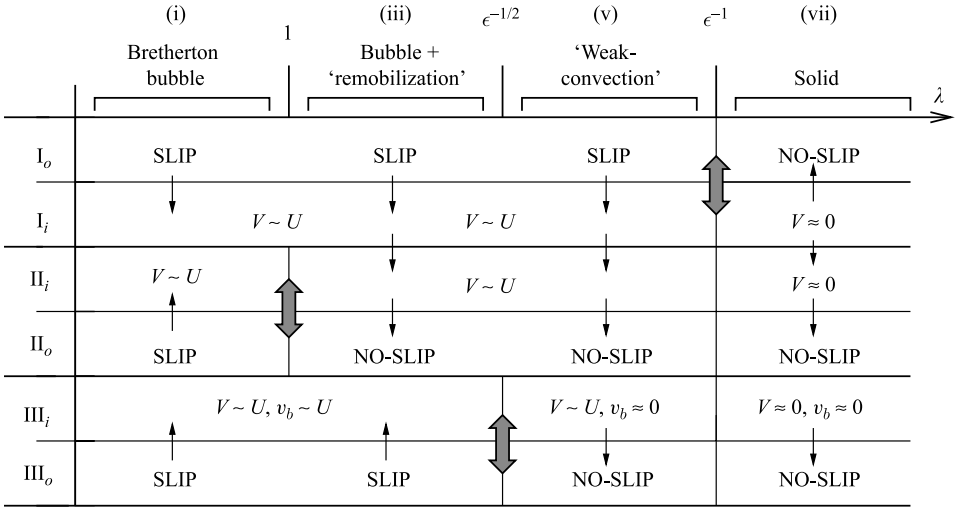

FIGURE 2. Summary of the interface boundary condition to be applied for each region of the drop. The viscosity ratio λ increases from left to right, defining cases (i)–(vii) as described in the text. Here, 'SLIP' implies stress-free, whereas 'NO-SLIP' implies that the boundary velocity is prescribed by the internal drop flow. Single-headed arrows show how the flow in one region drives (or modifies) the flow in an adjacent region; double-headed arrows denote a non-trivial coupling between flows in adjacent regions.

bubble U, and so

$$\epsilon = F(\lambda, Ca)\, Ca^{2/3} \tag{2.2}$$

for a film-thickness coefficient F of order unity that remains to be determined.

2.2. *Internal flow and velocity scales*

The interior and exterior flows may be coupled in each of regions I, II and III. We consider each case below.

2.2.1. *The region-I interface*

The cylindrical body of the drop (region I_i) has lengthscale R, and the interior velocity scale is V. The annular film has uniform thickness ϵR. Thus the stress in the film has magnitude $\mu(U-V)/(\epsilon R)$ that balances the internal stress $\lambda\mu V/R$. Thus the magnitude of the internal flow is $V \sim U/(1+\lambda\epsilon)$, that scales as U if $\lambda \ll \epsilon^{-1}$ and $U/\lambda\epsilon \ll U$ if $\lambda \gg \epsilon^{-1}$. Only when $\lambda\epsilon = O(1)$ are the flows in regions I_o and I_i fully coupled in the sense that both must be calculated simultaneously; $\lambda\epsilon$ is the interfacial mobility parameter (Davis, Schonberg & Rallison 1989) appropriate for the main body of the drop. This interaction of flows along the region-I interface is summarized in the top section of figure 2; the double-headed arrows show when the coupled problem arises.

2.2.2. *The region-II interface*

The internal stirring flow generated in the main body of the drop extends to the cap, so that $V \sim U$ for $\lambda \ll \epsilon^{-1}$. Both internal and external flows near the cap have lengthscale R. If $\lambda \ll 1$, internal stresses $\lambda\mu V/R$ are negligible in comparison with external stresses having magnitude $\mu U/R$. When $\lambda \sim 1$, internal and external stresses are comparable so the external flow is modified. When $1 \ll \lambda \ll \epsilon^{-1}$, the internal flow

has magnitude U and is unaffected by the flow in region II_o, but when $\lambda \gg \epsilon^{-1}$, the external flow past the cap is that past a drop with an effectively immobile interface.

The capillary number associated with the internal flow in the cap is $\lambda\mu V/\gamma$. Using the estimates above for V, this capillary number is no larger than $\epsilon^{-1}\mu U/\gamma = Ca^{1/3}$. Thus provided $Ca \ll 1$, the internal stress does not affect the cap shape, which remains hemispherical for all λ.

2.2.3. *The region-III interface*

The transition region III_o has lengthscale $\epsilon^{1/2}R$ that is small compared with the radius of the cap and of the tube. In consequence the interior Stokes flow in the region III_i is planar and equidimensional, extending a distance $\epsilon^{1/2}R$ into the drop interior. Furthermore for sufficiently small ϵ, this interior flow may be regarded as taking place in a half-space. The flow field therefore has two different lengthscales and the component of fluid velocity $u_b\boldsymbol{e}_z$ along the drop boundary may be written in the form

$$u_b(z) = -V + v_b(z); \tag{2.3}$$

here V varies on a lengthscale R, is determined by the full drop size and shape, and is approximately constant in the transition region, whereas v_b varies on the smaller lengthscale $\epsilon^{1/2}R$ and is generally negligible outside the transition region. The film-thickness coefficient F is determined in the transition region, and thus to find F we need only find the values of V and v_b.

Internal stresses in the transition region have magnitude $\lambda\mu V/(\epsilon^{1/2}R)$, and first become comparable with the shear stress $\mu U/(\epsilon R)$ in the film when $\lambda\epsilon^{1/2}$ is of order unity. This is the interfacial mobility parameter (Davis *et al.* 1989) for the transition region.

For $1 \ll \lambda \ll \epsilon^{-1/2}$ the region-III interface remains stress-free, the external flow is driven by the local curvature change and the film thickness is the same as that for $\lambda = 0$, implying the existence of a stagnation point on the interface in region III (Bretherton 1961). However, as we show below, a new asymptotic region appears between regions II and III in which the internal flow is coupled to that in the film, and over which the drop boundary velocity adjusts from the prescribed level $V \sim U$ in region II to the stress-free condition in region III (we term this effect 'remobilization', by analogy with surfactant-laden interfaces, as introduced by Stebe *et al.* 1991). The passive 'remobilization region' described in Appendix A has length R/λ (i.e. large compared with the transition region, but small compared with R). When $\lambda \sim 1$, the remobilization region merges with the cap region II; when $\lambda \sim \epsilon^{-1/2}$ it merges with region III. When $1 \ll \lambda \ll \epsilon^{-1/2}$, we show below that an additional stagnation point appears on the drop boundary in the remobilization region, approaching from the far field (region II) as λ increases.

When $\lambda\epsilon^{1/2}$ is of order unity, $V = U$ irrespective of the drop size and the internal flow in region III becomes fully coupled to that in the film. The associated internal fluid pressure has magnitude no larger than $\mu U/\epsilon R$ and this is a factor $\epsilon^{1/2}$ smaller than the capillary pressure γ/R. In consequence the scaling estimate (2.2) for ϵ is unaffected, but the coefficient F (of order unity) is a function of $\lambda\epsilon^{1/2}$. As $\lambda\epsilon^{1/2}$ increases through approximately 0.5, we show below that the two interfacial stagnation points merge, so that for sufficiently large λ the interfacial flow in region III is unidirectional.

When $\epsilon^{-1/2} \ll \lambda \ll \epsilon^{-1}$, again $V = U$ but now velocity variations along the transition region interface are suppressed and v_b has size $U/\lambda\epsilon^{1/2}$. The flow driven by the curvature change in region III extends a distance $\lambda\epsilon R$ into region I. This 'weak-convection

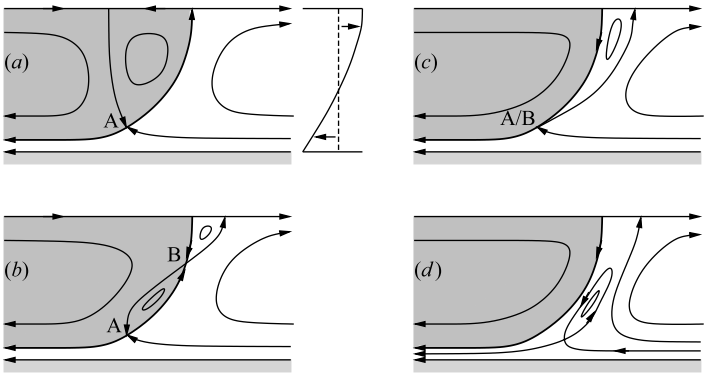

FIGURE 3. Sketches of approximate (and in cases *b–d*, proposed) streamline distributions for the low-Ca motion of (*a*) an inviscid bubble with $\lambda \ll 1$, for which there is a single intefacial stagnation point A; (*b*) a viscous drop with $1 \lesssim \lambda \ll \epsilon^{-1/2}$, showing an additional interfacial stagnation point B that approaches A as λ increases; (*c*) a viscous drop with $\lambda = O(\epsilon^{-1/2})$ for which A and B merge; (*d*) $\epsilon^{-1/2} \ll \lambda$.

region' is considered in Appendix B. It has no effect on the film thickness. When $\lambda \sim \epsilon^{-1}$, the weak-convection region merges with region I; when $\lambda \sim \epsilon^{-1/2}$ it merges with the transition region.

When $\lambda \sim \epsilon^{-1}$, the magnitude of V is $U/(1 + \lambda\epsilon)$, its precise value depending on the flow throughout the drop, and hence on the overall drop size. The film-thickness coefficient F remains of order unity but depends on $\lambda\epsilon$. Finally when $\lambda \gg \epsilon^{-1}$, the interior fluid has velocity of magnitude $U/\lambda\epsilon \ll U$, and the film thickness is that appropriate for a drop with an immobile surface.

2.3. *Flow patterns*

While we shall not explicitly compute flow patterns outside region III, sufficient is known from boundary conditions and topological constraints to sketch likely streamline distributions corresponding to the transitions described above. Figure 3(*a*) shows the well-known flow pattern around an inviscid drop ($\lambda \ll 1$)). A single 'Bretherton' stagnation point (A) lies on the drop interface in region III. The external flow in region II_o drives a recirculating flow in II_i, as demonstrated numerically by Westborg & Hassager (1989) and Martinez & Udell (1990). Once $1 \lesssim \lambda \ll \epsilon^{-1/2}$, the strengthening internal flow reduces the recirculation inside the drop and lowers the interfacial velocity until a second stagnation point appears on the interface, labelled B in figure 3(*b*). While our calculations below establish the existence of this second stagnation point for $1 \ll \lambda \ll \epsilon^{-1/2}$, we are not aware of computations in the literature confirming this proposed streamline distribution, nor are we confident of the precise nature of the topological transition between figures 3(*a*) and 3(*b*); in figure 3(*b–d*) we have sketched the simplest flow fields consistent with the available evidence, although other possibilities exist. As λ increases to $O(\epsilon^{-1/2})$, we show below that B moves into region III (as the 'remobilization' region shrinks) until A and B coincide (figure 3*c*). As λ increases further, mass conservation demands that the external flow is partially reversed where region II_o meets region III_o, since the thin film in region I_o can accommodate only a small proportion of the flux driven by the two converging interfaces. Thus a stagnation point moves into the interior of the fluid in region III_o, as sketched in figure 3(*d*). Ghadiali & Gaver's (2003) computations of low-Ca flow past a surfactant-covered bubble show similarly distorted streamlines near the bubble

tip, but we are not aware of numerical results directly identifying the proposed region of recirculating flow ahead of the bubble tip in figure 3(*d*).

2.4. *Summary of possible behaviours*

Seven asymptotic regimes may therefore be identified, as summarized in figure 2:

(i) if $\lambda \ll 1$, the drop behaves as an inviscid bubble;

(ii) if $\lambda \sim 1$, there is a non-trivial coupling between the flows in and around the cap (region II) but the film thickness is unaltered;

(iii) if $1 \ll \lambda \ll \epsilon^{-1/2}$, the film thickness is unaltered from Bretherton's (1961) $\lambda = 0$ value, but there is a passive 'remobilization region' over which the flow in the transition region matches on to the flow in the cap;

(iv) if $\lambda \sim \epsilon^{-1/2}$, there is a non-trivial coupling between the internal and external flows in the transition region III and the film thickness depends on $\lambda\epsilon^{1/2}$;

(v) if $\epsilon^{-1/2} \ll \lambda \ll \epsilon^{-1}$, the internal flow maintains the fluid velocity on the interface in the transition region as $V = U$, and there is a passive 'weak-convection region' that extends into the main body of the drop;

(vi) when $\lambda \sim \epsilon^{-1}$, there is a non-trivial coupling between the flows in regions I_i and I_o, and the film thickness depends on both $\lambda\epsilon$ and the overall drop shape;

(vii) if $\lambda \gg \epsilon^{-1}$ a slow internal flow is generated (with $V \sim U/\lambda\epsilon \ll U$), and the film thickness is that obtained by, for example, Schwartz *et al.* (1986) for an immobile interface.

3. Governing equations for the transition region

We continue to treat ϵ and λ as independent parameters and seek Ca via the $O(1)$ film-thickness coefficient F (see (2.2)). Scaling lengths on R, velocities on U and pressures on $(\mu U)/(\epsilon^{3/2}R)$, the Stokes equations for the external fluid are

$$\nabla \cdot \boldsymbol{u} = 0, \qquad \boldsymbol{0} = -\nabla p + \epsilon^{3/2}\nabla^2 \boldsymbol{u}. \tag{3.1}$$

At $r = 1$, $\boldsymbol{u} = -\boldsymbol{e}_z$. In addition, the velocity must match with the internal flow on $r = 1 - \epsilon h$. The normal stress condition may be written using (2.2) as

$$p_i - p + O\left(\lambda\epsilon^{3/2}V\right) = F^{3/2}\kappa, \tag{3.2}$$

where p_i is a constant internal pressure. The $O(\lambda\epsilon^{3/2}V)$ term arises from viscous stresses in the drop that are negligible.

The film thickness is set in the transition region III_o for which we write

$$z = -1 + \epsilon^{1/2}(x - x_0), \qquad r = 1 - \epsilon y, \tag{3.3}$$

for some constant x_0 of order unity determined in the far field. The coordinate system is shown in figure 4. Because ϵ is small, the governing equations for the film become those of lubrication theory, namely

$$-p_x + u_{yy} + O(\epsilon) = 0, \qquad p = p(x) + O(\epsilon) \qquad \text{for} \qquad 0 \leqslant y \leqslant h(x). \tag{3.4}$$

Using (3.2), the pressure gradient is $p_x = -F^{3/2}h_{xxx}$. The flow in the film is thus (using (2.3))

$$u(x, y) = -\tfrac{1}{2}F^{3/2}h_{xxx}y(y - h) + [-V + v_b(x)]\frac{y}{h} + \frac{y}{h} - 1, \tag{3.5}$$

with the associated flux $QU\epsilon R^2$ given by

$$Q = 2\pi \int_0^h u(x, y)\,\mathrm{d}y = 2\pi\left[\tfrac{1}{12}F^{3/2}h_{xxx}h^3 + \tfrac{1}{2}(-V + v_b(x) - 1)h\right]. \tag{3.6}$$

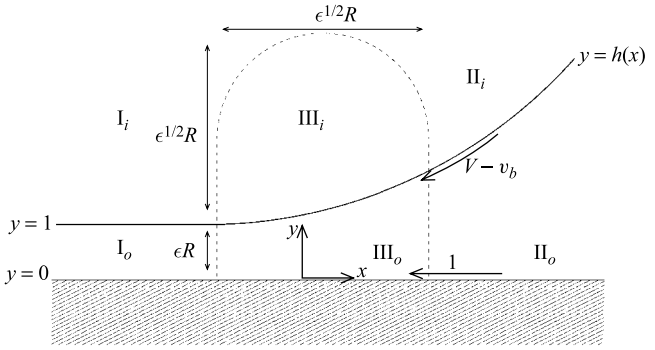

FIGURE 4. Sketch of the transition region at the front of the drop.

For a steady motion, Q is independent of x and, in the limit $x \to -\infty$, the transition region matches on to the constant-film-thickness region for which $h = 1$ and $v_b = 0$. Therefore $Q = -\pi(V + 1)$ and $h(x)$ is governed by a flux balance between the flow generated by surface tension and advection

$$\tfrac{1}{6}F^{3/2}h_{xxx}h^3 + (V + 1)(1 - h) + v_b h = 0, \tag{3.7}$$

with $h \to 1$ as $x \to -\infty$. As $x \to \infty$, the film matches on to the hemispherical cap and therefore $h \sim \frac{1}{2}x^2$. Furthermore, translational invariance implies that we may impose the additional condition $h \to \frac{1}{2}x^2 + O(1)$ as $x \to \infty$ so as to fix the origin x_0. For prescribed boundary velocities $v_b(x)$ and V, these conditions provide a unique solution for both $h(x)$ and F.

To close the problem we need $v_b(x)$ and V. This requires, in general, a determination of the internal flow, but some cases can be simplified. If $\lambda\epsilon^{1/2} \gg 1$ (cases (v)–(vii) in § 2.4), velocity variations along the transition region interface are suppressed, so that $v_b \approx 0$ and (3.7) becomes

$$\tfrac{1}{6}\,F^{3/2}\,h_{xxx}h^3 + (V + 1)(1 - h) = 0. \tag{3.8}$$

The constant velocity V is driven by shear stresses in region I and may be found by computing the internal flow on the tube radius scale R.

If $\lambda\epsilon \ll 1$ (cases (i)–(v) discussed in § 2.4), then V matches the wall velocity so that $V = 1$ and (3.7) becomes

$$\tfrac{1}{6}\,F^{3/2}\,h_{xxx}h^3 + 2(1 - h) + v_b\,h = 0, \tag{3.9}$$

and now we need only find $v_b(x)$ on the transition-region lengthscale $\epsilon^{1/2}R$. For this purpose we consider the shear stress exerted on the drop boundary, given by (3.5) as

$$f_b(x) = -u_y|_{y=h} = \tfrac{1}{2}\,F^{3/2}\,h_{xxx}h - v_b/h. \tag{3.10}$$

The $F^{3/2}$ term arises from the capillary-driven flow out of the film; the $-v_b/h$ term corresponds to the Couette flow that drives fluid into the film. When h is large ($x \to \infty$), the first dominates and $f_b > 0$, but when $h \approx 1$ ($x \to -\infty$) the second dominates, and $f_b < 0$. The flow in the transition region thus consists of a uniform velocity with $V = 1$, together with a locally varying flow v_b that is everywhere positive on the interface and (for $\lambda \gg 1$) tends to zero as $x \to \pm\infty$. We may use (3.7) in (3.10) to write instead

$$f_b(x) = -4v_b/h + 6(h - 1)/h^2. \tag{3.11}$$

Since $\epsilon \ll 1$, the interior flow in the transition region II_i may be regarded as two-dimensional and taking place in a half-space, so it is convenient to write $z = -1 + \epsilon^{1/2}(x - x_0)$, $r = 1 - \epsilon^{1/2} Y$. With velocity (relative to the local mean flow $-U\boldsymbol{e}_z$) and pressure scaled as before, we have

$$\nabla \cdot \boldsymbol{u} = 0, \qquad -\nabla p + \lambda \nabla^2 \boldsymbol{u} = \boldsymbol{0} \tag{3.12}$$

in $Y \geqslant 0$, where ∇ is now the gradient operator in the (x, Y)-plane. As $|\boldsymbol{x}| \to \infty$, $\boldsymbol{u} \to \boldsymbol{0}$. On $Y = 0$, the drop interface, the boundary condition is $\boldsymbol{u} \cdot \boldsymbol{n} = 0$. In addition, the tangential traction $f_b(x)$ must be related to the tangential velocity $v_b(x)$. This problem is well-suited to a boundary-integral method that we describe in Appendix C, which yields

$$f_b(x) = -\frac{2\lambda\epsilon^{1/2}}{\pi} \int_{-\infty}^{\infty} \frac{v_b(\xi) - v_b(x)}{(\xi - x)^2}\, \mathrm{d}\xi. \tag{3.13}$$

4. Results

We seek the solution of the problem defined by (3.9), (3.11), (3.13) and corresponding boundary conditions, from which we can determine the dependence of the film-thickness coefficient on the viscosity ration $\lambda\epsilon^{1/2}$. We begin by considering the limiting cases $\lambda\epsilon^{1/2} \ll 1$ and $\lambda\epsilon^{1/2} \gg 1$.

4.1. *Low-viscosity drops, $\lambda \ll \epsilon^{-1/2}$*

It is convenient to rescale (3.9) by setting $\xi = 3^{1/3} F^{-1/2} x$, so that

$$\tfrac{1}{2} h_{\xi\xi\xi} h^3 + 2(1 - h) + v_b\, h = 0. \tag{4.1}$$

The boundary conditions become

$$h \to 1 \quad \text{as} \quad \xi \to -\infty, \tag{4.2a}$$

$$h \to \tfrac{1}{2} 3^{-2/3} F\, \xi^2 + O(1) \quad \text{as} \quad \xi \to \infty. \tag{4.2b}$$

We have shown that if $\lambda \ll \epsilon^{-1/2}$ the drop boundary remains stress-free in region III so that $f_b = 0$. It follows from (3.11) that $v_b = 3(h - 1)/2h$. Therefore $v_b \to 0$ as $\xi \to -\infty$ and $v_b \to 3/2$ as $\xi \to \infty$, with a stagnation point ($v_b = 1$) when $h = 3$. Equation (4.1) then reduces to the Landau–Levich equation,

$$h_{\xi\xi\xi} h^3 + 1 - h = 0. \tag{4.3}$$

This widely studied equation has a unique solution with $F = F_0 \approx 1.337$ (Bretherton 1961).

For $1 \ll \lambda \ll \epsilon^{-1/2}$ there is a passive 'remobilization region,' examined in Appendix A, where the drop boundary mobilizes between the prescribed velocity in the cap (where $v_b = 0$) to the stress-free condition at the outer edge of the transition region (where $v_b = 3/2$). In addition to the stagnation point at $h = 3$, a second stagnation point appears a distance $5.6R/\lambda$ from the first (figure 10 in Appendix A). Between the two, there is a reverse flow along the drop interface; the likely streamline pattern is sketched in figure figure 3(*b*). The film thickness is unaffected to leading order.

4.2. *High-viscosity drops, $\lambda \gg \epsilon^{-1/2}$*

Writing $\xi = 6^{1/3} F^{-1/2} (V + 1)^{1/3} x$ recasts (3.8) in the Landau–Levich form (4.3). The boundary conditions become

$$h \to 1 \quad \text{as} \quad \xi \to -\infty, \tag{4.4a}$$

$$h \to \tfrac{1}{2} 6^{-2/3} (V + 1)^{-2/3} F\, \xi^2 + O(1) \quad \text{as} \quad \xi \to \infty, \tag{4.4b}$$

and so the film thickness is $F = 2^{2/3}F_0(V+1)^{2/3}$. In general V can be determined only by finding the flow in the body of the drop numerically. However, in two cases V is known explicitly. When $\epsilon^{-1/2} \ll \lambda \ll \epsilon^{-1}$ the boundary moves with the same speed as the wall so that $V = 1$; and if $\lambda \gg \epsilon^{-1}$, the drop boundary becomes immobile so that $V = 0$. In the latter case (labelled (vii) in § 2.4), the film thickness is $F_\infty = 2^{2/3}F_0 \approx 2.123$. For the 'plateau regime' (labelled (v) in § 2.4) the film is even thicker, with $F = F_P = 4^{2/3}F_0 \approx 3.370$. For a drop whose surface has been partially rigidified by surfactant the same result has been obtained by Ratulowski & Chang (1990).

When $\lambda \sim \epsilon^{-1}$, we can estimate V by calculating the speed of the fluid at the cylindrical interface away from the ends of the drop. The flow in the main body of the drop is unidirectional and there is no net flux of fluid. In consequence, $u = V(1-2r^2)$. In the annular film, the flow is Couette with $u = (1-V)(1-r)/\epsilon - 1$. Balancing tractions at the interface we obtain $V = 1/(1+4\lambda\epsilon)$. This gives the estimate

$$F \approx 2^{2/3}F_0\left(\frac{2+4\lambda Ca^{2/3}F}{1+4\lambda Ca^{2/3}F}\right)^{2/3}, \tag{4.5}$$

though since within an order-R distance of the end of the drop the internal flow is not unidirectional, this result is not exact. Results showing F as a function of λ and Ca (decreasing monotonically from F_P to F_∞ as each increases) are shown in figure 9 below.

4.3. *Intermediate-viscosity drops, $\lambda \sim \epsilon^{-1/2}$*

When $\lambda \sim \epsilon^{-1/2}$, the coupled equations (3.9), (3.11), (3.13) for $h(x)$, $f_b(x)$ and $v_b(x)$ must be solved for the transition region. After writing $\xi = 6^{1/3}\,F^{-1/2}\,x$, these equations become

$$h_{\xi\xi\xi}h^3 + 2(1-h) + v_b\,h = 0, \tag{4.6a}$$

$$f_b(\xi) = -\frac{4v_b}{h} + \frac{6(h-1)}{h^2} = -\tilde{\lambda}\fint_{-\infty}^{\infty}\frac{v_b(\tilde{\xi}) - v_b(\xi)}{(\tilde{\xi}-\xi)^2}\,\mathrm{d}\tilde{\xi}, \tag{4.6b}$$

where the the inverse interface mobility parameter (Davis *et al.* 1989) is $\tilde{\lambda} = 2\lambda 6^{1/3}\epsilon^{1/2}/\pi F^{1/2} = 2(6Ca)^{1/3}\lambda/\pi$. The boundary conditions are

$$\begin{gathered} v_b \to 0, \quad h \to 1 \quad \text{as} \quad \xi \to -\infty, \\ v_b \to 0, \quad h \to \frac{1}{2}6^{-2/3}F\xi^2 + O(1) \quad \text{as} \quad \xi \to \infty. \end{gathered} \tag{4.6c}$$

4.3.1. *Far-field estimates*

Before embarking on a numerical solution of (4.6*a–c*), we consider the far-field limits. On integrating by parts, (4.6*b*) gives

$$f_b(\xi) = -\tilde{\lambda}\fint_{-\infty}^{\infty}\frac{v_b'(\tilde{\xi})}{\tilde{\xi}-\xi}\,\mathrm{d}\tilde{\xi}, \tag{4.7}$$

a Hilbert transform with inverse

$$v_b(\xi) = -\frac{1}{\pi^2\tilde{\lambda}}\fint_{-\infty}^{\infty} f_b(\tilde{\xi})\,\ln|\tilde{\xi}-\xi|\,\mathrm{d}\tilde{\xi}. \tag{4.8}$$

The leading-order term in f_b as $\xi \to \infty$ is, from (4.6*b*), $12\ 6^{2/3}/F\xi^2$, so in this limit (4.7) becomes

$$\frac{12\ 6^{2/3}}{F\xi^2} = -\tilde{\lambda}\int_{-\infty}^{\infty} \frac{v_b'(\tilde{\xi})}{\tilde{\xi}-\xi}\,\mathrm{d}\tilde{\xi}, \tag{4.9}$$

indicating that for small $\tilde{\lambda}$ and large ξ an outer region of length $\tilde{\lambda}^{-1}$ appears, over which v_b adjusts from 3/2 to zero. This is the 'remobilization region' considered in Appendix A. For non-zero $\tilde{\lambda}$, the leading-order behaviour of v_b in the limit $\xi \to \infty$ comes from the corresponding far-field behaviour of f_b, and (4.8) gives

$$v_b \sim \left(12\ 6^{2/3}/\pi^2 F\tilde{\lambda}\right)\ \ln(\xi)/\xi + O(1/\xi) \qquad \text{as} \qquad \xi \to \infty. \tag{4.10}$$

Thus v_b decays slightly more slowly than the velocity generated by a two-dimensional force dipole.

For non-zero $\tilde{\lambda}$, the kernel in (4.6*b*) generates algebraic decay in v_b as $\xi \to -\infty$. In consequence (4.6*a*) implies that there is also algebraic decay of h as $\xi \to -\infty$, rather than the exponential decay encountered in (4.3). Thus from (4.6*a*, *b*) we have $h = 1 + v_b/2$, $f_b = -v_b$ as $\xi \to -\infty$. The total force that can be applied by the film to the drop is zero, so

$$\int_{-\infty}^{\infty} f_b(\xi)\ \mathrm{d}\xi = 0. \tag{4.11}$$

If this integral is to remain finite we certainly need $f_b = o(1/\xi)$ and hence also $v_b = o(1/\xi)$ as $\xi \to -\infty$.

For large $\tilde{\lambda}$, (4.8) implies that v_b is of magnitude $\tilde{\lambda}^{-1}$. Thus, in order that the total force remains zero, v_b must decay on a lengthscale $\tilde{\lambda}$ as $\xi \to -\infty$. This is the 'weak-convection region' discussed in Appendix B, where we show that v_b decays like $(\xi \ln|\xi|)^{-2}$ as $\xi \to -\infty$.

4.3.2. *Numerical method*

Surface points ξ_i $(i = 1, \ldots, n)$ equally spaced along the region-III interface were chosen (typically $\xi_1 = -20$, $\xi_n = 80$, $n = 1000$), and the integral in (4.6*b*) was evaluated between ξ_1 and ξ_n using the trapezoidal rule so as to reduce the integral equation to a matrix equation for the velocities $v_b(\xi_i)$ $(i = 1, \ldots, n)$. This equation may be solved by Gaussian elimination, using the $\lambda = 0$ solution for $h(\xi)$ as a first guess on the right-hand side. This gives v_b, and (4.6*a*) provides an improved estimate for $h(\xi)$. The differential equation may be solved using a shooting method, starting from $\xi = \xi_1 < 0$ with

$$h = 1 + \tfrac{1}{2}v_b(\xi_1) + A\exp\left(2^{1/3}\xi_1\right), \tag{4.12}$$

for some constant A and v_b obtained from the previous iteration. This Picard iteration for v_b and h converges to two significant figures in about ten iterations.

We removed the singular behaviour at $\tilde{\xi} = \xi$ by integrating up to $\xi - \delta$ (for some $\delta \ll 1$) and then from $\xi + \delta$ onward, checking that the size of δ has no effect on the results for F.

Since $v_b \to 0$ as $\xi \to \pm\infty$, we began by taking $v_b = 0$ outside the numerical domain, i.e. we estimated the contribution to the integral in (4.6*b*) for $\xi > \xi_n$ as

$$\tilde{\lambda}\int_{\xi_n}^{\infty} \frac{v_b(\xi)}{(\tilde{\xi}-\xi)^2}\ \mathrm{d}\tilde{\xi} = \tilde{\lambda}\frac{v_b(\xi)}{\xi_n - \xi},$$

and equivalently for $\xi < \xi_1$. As can be seen from figure 5(*a*) for $\tilde{\lambda} = 1$, this method is inaccurate because the decay of v_b as $\xi \to \infty$ is slow. Errors are even greater for

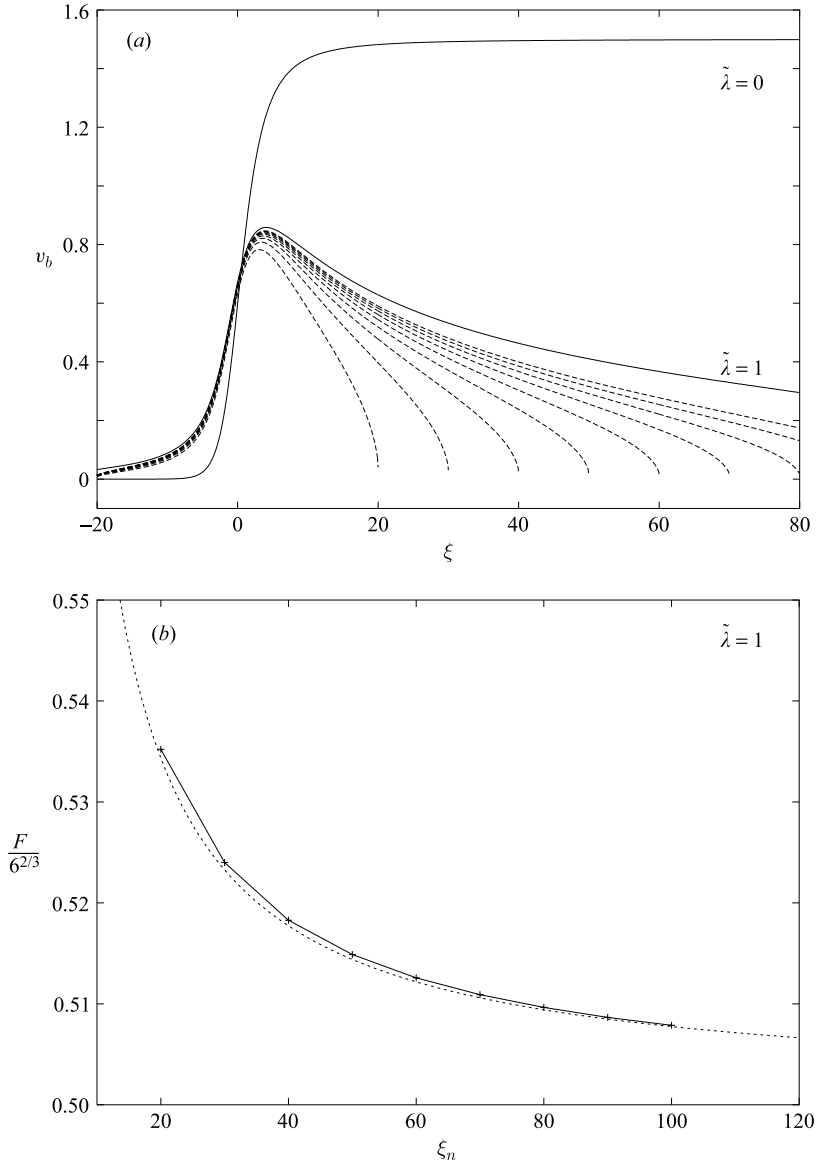

FIGURE 5. Effect of domain size for $\tilde{\lambda}=1$, taking $v_b=0$ outside the numerical domain $(-20, \xi_n)$, for $\xi_n=20, 30, 40, 50, 60, 70, 80, 90, 100$. (*a*) Velocity v_b; solid lines show the known solution for $\tilde{\lambda}=0$ and the result for $\tilde{\lambda}=1$ extrapolated to $\xi_n=\infty$; dashed lines show for each finite domain size the results for $\tilde{\lambda}=1$. (*b*) Film-thickness coefficient $F/6^{2/3}$ for $\tilde{\lambda}=1$. The dashed curve is the numerical fit $0.501+0.67/\xi_n$, suggesting that for a numerical domain of infinite length $F/6^{2/3}=0.501$.

large or small $\tilde{\lambda}$, since the decay takes place over a length $\tilde{\lambda}$ or $\tilde{\lambda}^{-1}$ respectively that is not captured. We were able, however, to obtain estimates for F by extrapolation, as shown in figure 5(*b*), and also to confirm that v_b does decay at a rate comparable to $1/\xi$ as $\xi\to\infty$ and to $1/\xi^2$ as $\xi\to-\infty$.

To improve the accuracy, we included additional terms in the far-field representation of v_b. For a finite range the logarithm in (4.10) is indistinguishable from a constant, so

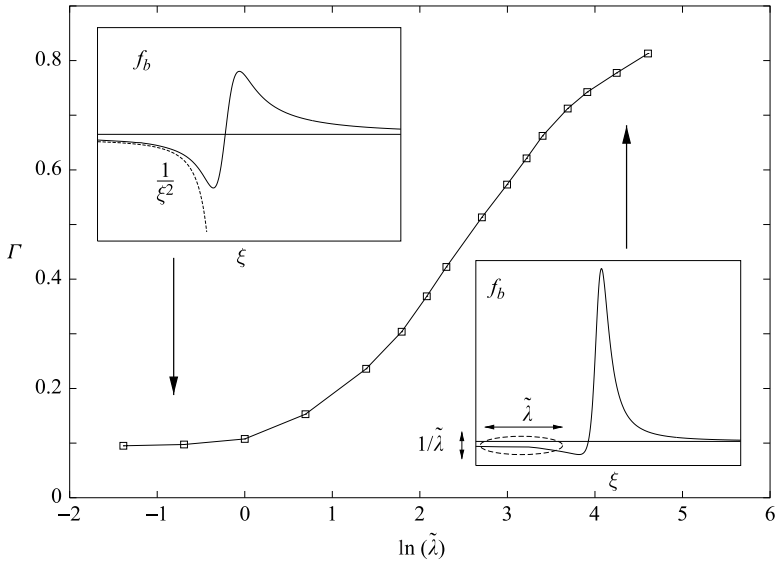

FIGURE 6. Error estimate Γ defined by (4.13), for a numerical domain $-20 \leqslant \xi \leqslant 80$. The insets show the behaviour of the tail of f_b as $\xi \to -\infty$.

we put $v_b(\xi) = B_>/\xi$ for $\xi > \xi_n$, with the coefficient $B_>$ determined from the previous iteration. The contribution to the integral (4.6*b*) for $\xi > \xi_n$ may then be estimated as

$$\tilde{\lambda} B_> \left(\frac{1}{\xi^2} \ln \left(\frac{\xi_n}{\xi_n - \xi} \right) - \frac{1}{\xi(\xi_n - \xi)} \right) + \tilde{\lambda} \frac{v_b(\xi)}{\xi_n - \xi}.$$

Similarly, writing $v_b(\xi) = B_</\xi^2$ for $\xi < \xi_1$ gives a contribution to the integral for $\xi < \xi_1$ as

$$\tilde{\lambda} B_< \left(\frac{2}{\xi^3} \ln \left(\frac{\xi_1 - \xi}{\xi_1} \right) + \frac{2\xi_1 - \xi}{\xi^2 \xi_1 (\xi_1 - \xi)} \right) - \tilde{\lambda} \frac{v_b(\xi)}{\xi_1 - \xi}.$$

Using this method we were able to find results for F correct to two significant figures for a domain $(-20, 80)$ and $n = 1000$. We reproduced these results over the domain $(-256, 256)$ by using a relaxation method to determine h on an exponentially stretched ξ-grid, using a linear approximation for v_b on each integration panel. Further details of the numerical scheme are provided in Hodges (2003).

A test of the accuracy of the results is that the total force on the drop should be zero. Figure 6 shows calculated values of

$$\Gamma = \int_{-\infty}^{\infty} f_b(\xi) \mathrm{d}\xi \Big/ \int_{-\infty}^{\infty} |f_b(\xi)| \mathrm{d}\xi, \tag{4.13}$$

for $\tilde{\lambda}$ between $\frac{1}{4}$ and 100, and a numerical range $-20 \leqslant \xi \leqslant 80$. The results suggest typical errors of 10% in f_b, increasing with $\tilde{\lambda}$. The reason for the increasing error is that we do not capture the long tail of size $\tilde{\lambda}$ when $\tilde{\lambda}$ is large (see figure 6). The errors are halved on a domain $(-256, 256)$. Surprisingly, these errors at large $\tilde{\lambda}$ do not significantly affect the film-thickness coefficient F: when $\tilde{\lambda}$ is large, v_b is small and so has only a small effect on h.

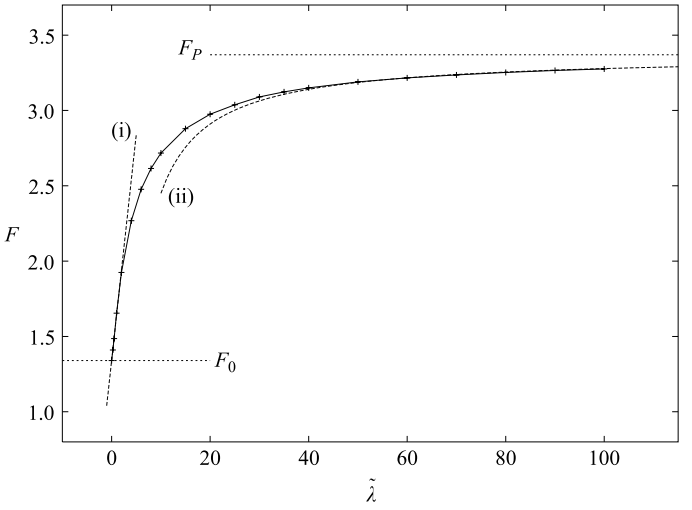

FIGURE 7. Film thickness F as a function of $\tilde{\lambda} = 2(6Ca)^{1/3}\lambda/\pi$. Dashed curves show the numerical fits: (i) $F_0 + 0.3\,\tilde{\lambda}$ and (ii) $F_P - 9.2/\tilde{\lambda}$.

4.3.3. *Numerical results*

Solutions to (4.6*a–c*) were computed for values of $\tilde{\lambda}$ between $\frac{1}{4}$ and 100. Figure 7 shows the film-thickness coefficient F, which in this parameter regime is monotone increasing with $\tilde{\lambda}$.

Figure 8 shows, for each value of $\tilde{\lambda}$, v_b and f_b along the transition-region interface. As $\tilde{\lambda} \to 0$, v_b resembles the velocity distribution for $\lambda = 0$, except that at large ξ, v_b decays like $\ln(\xi)/\xi$ over a lengthscale $\tilde{\lambda}^{-1}$. This is the 'remobilization' discussed in Appendix A.

As $\tilde{\lambda}$ increases, v_b falls, but the traction f_b increases near $\xi = 0$; $v_b(\xi)$ is everywhere less than 1 when $\tilde{\lambda} \gtrsim 0.5$ and thus, as shown by (3.5), the stagnation points on the drop merge and one moves into the fluid, as sketched in figure 3(*c*, *d*). As $\tilde{\lambda} \to \infty$, f_b consists of a (finite) positive traction near $\xi = 0$, together with a weak negative traction in $\xi < 0$ where f_b remains of magnitude $\tilde{\lambda}^{-1}$ over a distance $\tilde{\lambda}$. This is the 'weak-convection' regime discussed in Appendix B.

5. Discussion

We have investigated the effect of drop viscosity on the film thickness surrounding a drop moving steadily through a cylindrical tube. In all cases, the film thickness ϵ scales as $Ca^{2/3}$ for $Ca \ll 1$. We anticipate that the same methods of asymptotic and numerical analysis will also be appropriate in other coating problems involving the interaction of a viscous fluid with a thin layer of a relatively inviscid fluid.

As is well-known (Schwartz *et al.* 1986), the film surrounding a near-rigid drop ($\lambda \to \infty$) is thicker by a factor of $2^{2/3}$ than for an inviscid bubble ($\lambda = 0$). Previous experiments and computations for surfactant-free systems (e.g. Fairbrother & Stubbs 1935; Taylor 1961; Goldsmith & Mason 1963; Martinez & Udell 1990) have suggested either a monotonic increase in the film-thickness coefficient F from F_0 to F_∞, or else were unable to detect a significant dependence of F on λ (Chen 1986; Westborg & Hassager 1989). We have shown here that for intermediate values of λ, the film can be thicker by up to a factor $4^{2/3}$. The theory presented in this paper is formally valid in

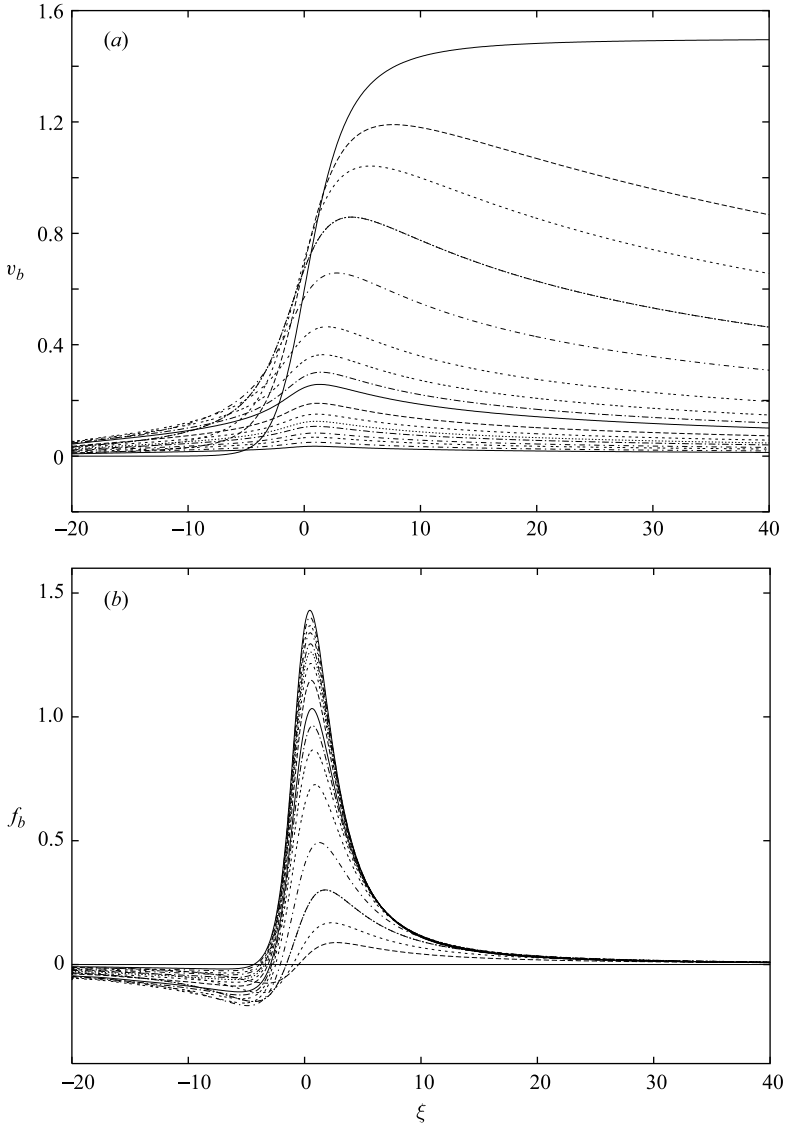

FIGURE 8. Numerical solutions to (4.6*a*, *b*) showing (*a*) velocity v_b; (*b*) shear traction f_b along the transition region interface. Results shown for $\tilde{\lambda} = 0, \frac{1}{4}, \frac{1}{2}, 1, 2, 4, 6, 8, 10, 15, 20, 25, 30, 40, 50, 70$ and 100. The case $\tilde{\lambda} = 0$ is the top curve in (*a*) and the bottom curve in (*b*).

the limit $Ca \to 0$ for which the viscosity ratios $Ca^{-1/3}$ and $Ca^{-2/3}$ are well-separated, and in that limit a plateau appears. Figure 9 shows F as a function of viscosity ratio for (*a*) $Ca = 10^{-21}$, (*b*) $Ca = 10^{-12}$ and (*c*) $Ca = 10^{-3}$. In each case the curve shown is a 'patch' of the theories for $\lambda Ca^{1/3} \sim 1$ shown in figure 7 together with that for $\lambda Ca^{2/3} \sim 1$ from (4.5). Somewhat disappointingly, the results indicate that to observe a well-defined plateau experimentally would require a capillary number as small as $Ca = 10^{-18}$ with λ in the range 10^6 to 10^{12}. For more accessible capillary numbers (e.g. $Ca = 10^{-3}$) the $\lambda Ca^{1/3} = O(1)$ and $\lambda Ca^{2/3} = O(1)$ regimes overlap, so that the predicted maximum film thickness is only a little greater than F_∞ — the figure

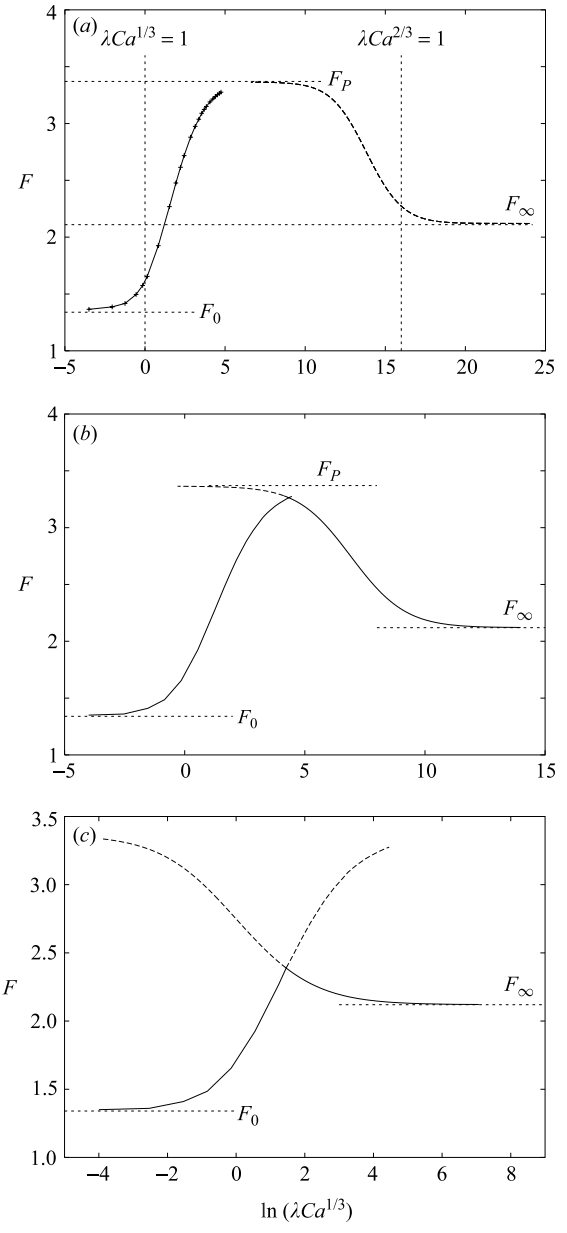

FIGURE 9. Film thickness: results showing F as a function of $\lambda \mathrm{Ca}^{1/3}$ (left, as in figure 7) and of $\lambda \mathrm{Ca}^{2/3}$ (right, as in (4.5)) for (*a*) $Ca = 10^{-21}$; (*b*) $Ca = 10^{-12}$; and (c) $Ca = 10^{-3}$. Also shown are the asymptotes $F_0 \approx 1.34$, $F_P \approx 3.37$ and $F_\infty \approx 2.12$.

suggests by about 12%. Furthermore, this overshoot may only be observed over a limited range of λ, approximately $30 < \lambda < 100$. For Ca sufficiently large (> 0.1), the film thickness increases monotonically from F_0 to F_∞ (Martinez & Udell 1990). We do not know the value of Ca at which the maximum disappears.

Experimental and computational studies are needed to corroborate the existence of a plateau and overshoot in film thickness and to determine how small Ca needs to be for an overshoot to appear. A number of experimental difficulties are likely to arise

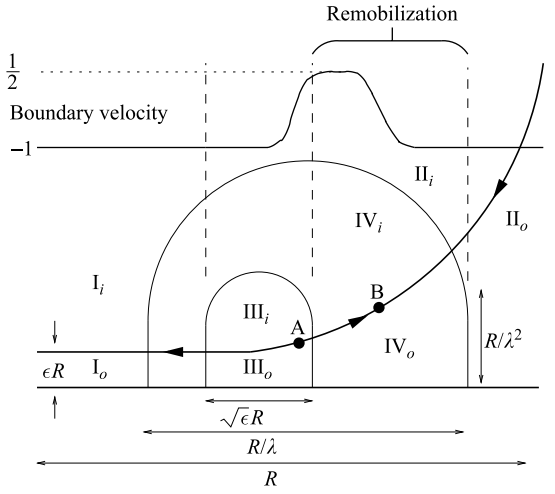

FIGURE 10. Sketch showing the remobilization region for $1 \ll \lambda \ll \epsilon^{-1/2}$. A and B correspond to the stagnation points sketched in figure 3(*b*).

in such an investigation. First, λ must be large, and therefore a long time (or a long tube) is needed to establish an equilibrium film thickness. Second, for small values of *Ca* the film is thin, leading to possible rupture (or film thickening) by van der Waals forces (Teletzke, Davis & Scriven 1988). Third, readjustment of the film over long lengthscales via coupling to the core flow may also be significant (Cachile *et al.* 1996). Fourth, surfactant impurities are hard to eliminate and are likely to complicate the observed behaviour. Nevertheless we hope that this paper will stimulate such experiments. In addition, the complex streamline patterns of § 2 that we have, in part, conjectured merit further investigation; they present a difficult computational challenge in view of the disparity in lengthscales involved.

S. R. H. acknowledges with gratitude a Research Studentship from the EPSRC.

Appendix A. Remobilization regime for $1 \ll \lambda \ll \epsilon^{-1/2}$

If $1 \ll \lambda \ll \epsilon^{-1/2}$ the drop boundary in region III_0 is stress-free and its velocity is given by $u_b = -1 + v_b$, $v_b = 3(h-1)/2h$. Thus as $h \to \infty$, $u_b = \frac{1}{2}$, as for the inviscid Bretherton problem. However, the fluid velocity along the drop boundary in region II_0 is driven by stirring within the drop, on a lengthscale comparable with the tube radius. Near the tube wall in region II_0, therefore, $u_b = -1$. It follows that a 'remobilization region' appears (labelled region IV in figure 10) between regions II and III, within which v_b varies between 0 and $\frac{3}{2}$. Region IV has $O(1)$ aspect ratio and has region III embedded within it.

We denote the horizontal length of region IV by $\mathscr{L}R$, for some $\epsilon^{-1/2} \ll \mathscr{L} \ll 1$. The greatest film thickness in region IV_o is then $\mathscr{L}^2 R$. Stresses within the drop have magnitude $\lambda\mu U/\mathscr{L}R$, balanced by film stresses $\mu U/\mathscr{L}^2 R$. It follows that $\mathscr{L} \sim 1/\lambda$. When $\lambda \sim \epsilon^{-1/2}$ the remobilization region merges with the transition region III; when $\lambda \sim 1$ the remobilization region merges with the cap in region II.

For region IV_o we write $z = -1 + X/\lambda$ and consider the outer limit of region III_o, so that the dimensional stress along the interface is $\mu U \lambda^2 f_b/R$, where, from (3.11)

$$f_b(X) = H(X)(12 - 8v_b)/X^2, \tag{A 1}$$

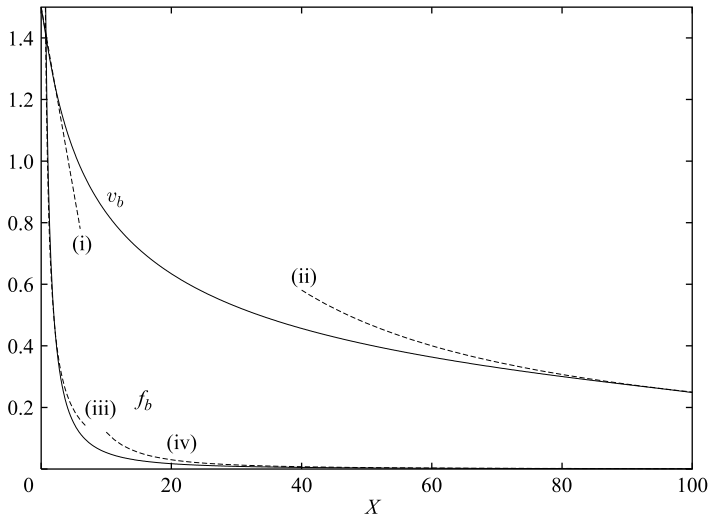

FIGURE 11. Numerical solution to remobilization problem (A 4). Dashed curves show (i) $3/2 - 3X/8\pi$; (ii) $6\ln X/\pi X + 16.2/X$; (iii) $3/\pi X$; (iv) $12/X^2$.

with $H(X)$ a Heaviside function. Then the boundary-integral representation (3.13) gives, in $X \geqslant 0$,

$$f_b(X) = \frac{12 - 8v_b}{X^2} = -\frac{2}{\pi}\fint_{-\infty}^{\infty} \frac{v_b(\tilde{X}) - v_b(X)}{(\tilde{X} - X)^2}\,\mathrm{d}\tilde{X}, \tag{A 2}$$

with inverse (4.8)

$$v_b(X) = -\frac{1}{2\pi}\fint_0^{\infty} f_b(\tilde{X})\ \ln|\tilde{X} - X|\,\mathrm{d}\tilde{X} \qquad (X \geqslant 0). \tag{A 3}$$

Now $v_b = 0$ for $X < 0$, and so in $X > 0$

$$f_b(X) = \frac{12 - 8v_b(X)}{X^2} = \frac{2}{\pi}\frac{v_b(X)}{X} - \frac{2}{\pi}\fint_0^{\infty} \frac{v_b(\tilde{X}) - v_b(X)}{(\tilde{X} - X)^2}\,\mathrm{d}\tilde{X}. \tag{A 4}$$

Thus $v_b \to 0$ as $X \to \infty$ and

$$f_b(X) \sim \frac{3}{\pi X}, \qquad v_b(X) \sim \frac{3}{2} - \frac{3X}{8\pi} \qquad \text{as} \qquad X \to 0+. \tag{A 5}$$

Equation (A 4) may be solved over a numerical domain $[\delta, X_n]$ for some $\delta \ll 1$ and $X_n \gg 1$. Using (A 5), the contribution to the integral (A 4) for $0 \leqslant X \leqslant \delta$ is

$$\frac{3}{8\pi}\left(\frac{X}{\delta - X} - \ln(X - \delta) + 1 + \ln X\right) - \left(\frac{3}{2} - v_b(X)\right)\left(\frac{1}{\delta - X} + \frac{1}{X}\right).$$

Since $f_b \sim 12/X^2$ as $X \to \infty$, (A 3) gives $v_b(X) = 6\ln X/(\pi X) + O(1/X)$ as $X \to \infty$. Approximating v_b as $v_b(X) = B_>/X$ for $X \geqslant X_n$, the contribution to the integral in (A 4) for $X \geqslant X_n$ is

$$\frac{2B_>}{\pi}\left(\frac{1}{X^2}\ln\left(\frac{X_n}{X_n - X}\right) - \frac{1}{X(X_n - X)}\right) + \frac{2}{\pi}\frac{v_b(X)}{X_n - X}.$$

Equation (A 4) may now be solved iteratively, updating $B_>$ at each iteration until its value is unchanged to two significant figures; this takes about ten iterations. The accuracy of the solutions presented in figure 11 was checked by varying the values

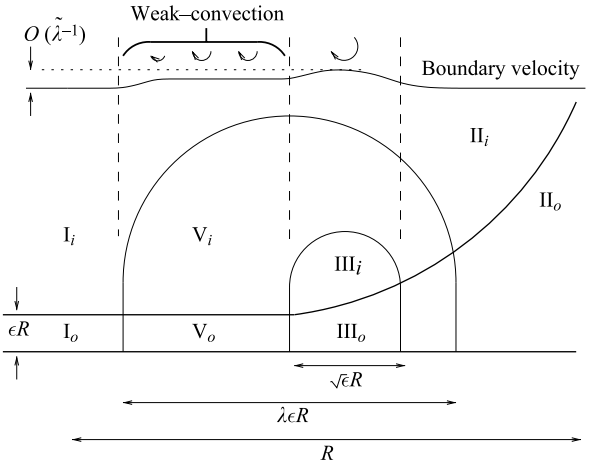

FIGURE 12. Sketch showing the weak-convection region for $\epsilon^{-1/2} \ll \lambda \ll \epsilon^{-1}$.

of δ and X_n. As shown in figure 11, $v_b = 1$ at $X \approx 5.6$. Therefore, the 'Bretherton' stagnation point (labelled A in figures 3(*b*) and 10) on the interface at $X = 0$ and the 'remobilization' stagnation point on the interface (B in figure 10) are separated by a distance $5.6R/\lambda$. The singular behaviour of f_b as $X \to 0+$ in (A 5) arises from the abrupt change in v_b across region III; this is smoothed by an 'inner' solution in region III.

Appendix B. Weak–convection regime for $\epsilon^{-1/2} \ll \lambda \ll \epsilon^{-1}$

When $\tilde{\lambda} \sim \lambda\epsilon^{1/2} \gg 1$, the interfacial velocity in the transition region III differs from U by a small correction v_b of dimensional size $\tilde{\lambda}^{-1}U$. This velocity difference induces a shear stress in the film of size $\mu\, v_b/\epsilon R$, balanced by an internal stress that scales as $\lambda\mu\, v_b/\mathscr{L}$, where $\mathscr{L} \sim \lambda\epsilon R$ is the associated lengthscale. Thus a new 'weak-convection region' (labelled region V in figure 12) appears between regions I and III. It merges with the transition region III when $\lambda \sim \epsilon^{-1/2}$, and with the flow on the lengthscale of the tube when $\lambda \sim \epsilon^{-1}$. The flow is driven by the rapid curvature change that takes place in the relatively small region III.

We may examine the parameter regime $\epsilon^{-1/2} \ll \lambda \ll \epsilon^{-1}$ by considering (4.6*a*) and (4.6*b*) in the limit $\tilde{\lambda} \to \infty$. At leading order, $v_b = 0$ so that

$$h_{\xi\xi\xi}h^3 + 2(1-h) = 0, \qquad f_b = 6(h-1)/h^2. \tag{B 1}$$

The film thickness then has the 'plateau value' F_p. Furthermore, the total force applied to the drop which arises from shear stresses induced by surface tension in region III is

$$\mathscr{F}_b \equiv \int_{-\infty}^{\infty} f_b(\xi)\ \mathrm{d}\xi = 6\int_{-\infty}^{\infty} (h-1)/h^2\ \mathrm{d}\xi \approx 8.8. \tag{B 2}$$

This force is balanced by a shear stress of magnitude $\tilde{\lambda}^{-1}$ acting over a distance $\tilde{\lambda}$ in the weak-convection region, for which we write $X = \xi/\tilde{\lambda}$. On this long lengthscale, (4.6*a*) becomes $h = 1 + v_b/2$, and therefore $f_b = -v_b$ in $X < 0$, with $f_b = 0$ in $X > 0$. This stress in $X < 0$ results from a Couette flow in the film; the contribution from surface tension is negligible since the drop boundary is flat. The force balance implies

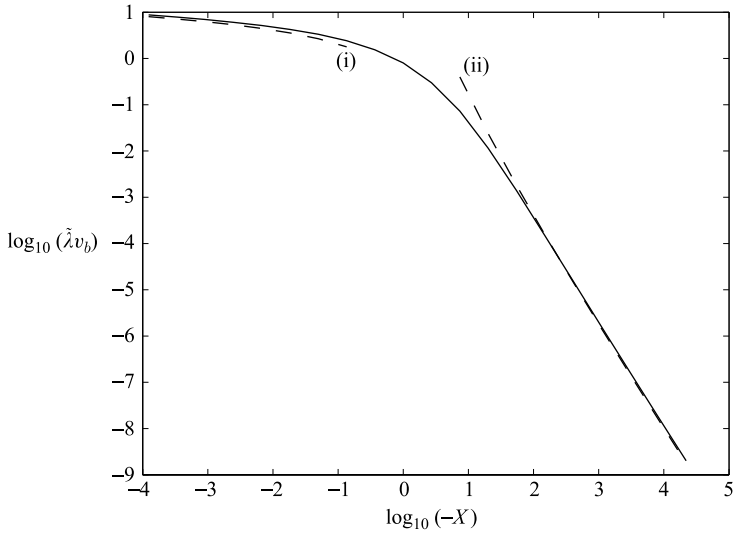

FIGURE 13. Boundary velocity for the weak-convection regime. Dashed curves show (i) $\tilde{\lambda}\, v_b = -8.8\, \ln|X|/\pi^2$; (ii) $\tilde{\lambda}\, v_b = 8.8\, (\pi/X \ln|X|)^2$.

that

$$\int_{-\infty}^{0} v_b \, \mathrm{d}X = \mathscr{F}_b/\tilde{\lambda}. \tag{B 3}$$

On this scale the region-III force becomes a δ-function concentrated at $X=0$, so $f_b = \mathscr{F}_b\delta(X) - v_b(X)H(-X)$. The boundary velocity $v_b(X)$ satisfies the integral equation (4.8), so that, using (B 3),

$$v_b(X) - \frac{1}{\pi^2}\int_{-\infty}^{0} v_b(\tilde{X}) \ln|\tilde{X} - X| \, \mathrm{d}\tilde{X} = -\frac{\mathscr{F}_b}{\pi^2\tilde{\lambda}} \ln|X|. \tag{B 4}$$

An explicit form for $v_b(X)$ may be obtained by using Laplace transforms for the convolution integral and a Hankel inversion contour for the logarithmic branch cut, giving

$$\tilde{\lambda}\; v_b(X) = \mathscr{F}_b\pi^2 \int_0^{\infty} s\, \mathrm{e}^{sX} \Big/ \left[(\ln s + \gamma - \pi^2 s)^2 + \pi^2\right] \, \mathrm{d}s, \qquad X < 0, \tag{B 5}$$

where γ is Euler's constant. Asymptotic forms are

$$\begin{aligned} \tilde{\lambda}\; v_b(X) &\sim -\mathscr{F}_b \ln|X|/\pi^2, \quad X \to 0 \\ &\sim \mathscr{F}_b(\pi/X \ln|X|)^2, \quad X \to -\infty. \end{aligned} \tag{B 6}$$

The function $\tilde{\lambda}\, v_b$ is shown on in figure 13. The singular behaviour at $X=0$ is smoothed by an inner solution in region III, and corresponds to the point force seen by the outer flow in region V. The behaviour at $X \to -\infty$ is determined by the asymptotic behaviour $f_b = -v_b$ in the far field. As shown in figure 13, the asymptote is attained only for $X < -100$.

Appendix C. Boundary-integral formulation for a planar Stokes flow

Consider a Stokes flow of a fluid having viscosity $\lambda\mu$ in a connected planar region with smooth boundary ∂S and outward normal $\boldsymbol{n}$. The conventional integral

representation of such a flow gives the velocity $\boldsymbol{u}$ at a point $\boldsymbol{x}_0$ as an integral that involves $\boldsymbol{u}$ on the boundary and the surface traction $\boldsymbol{f} = \boldsymbol{\sigma} \cdot \boldsymbol{n}$ (variables in this Appendix are dimensional). Specifically (Pozrikidis 1992),

$$\chi(\boldsymbol{x}_0)\, \boldsymbol{u}(\boldsymbol{x}_0) \;=\; \fint_{\partial S} [\boldsymbol{J}(\boldsymbol{R}) \cdot \boldsymbol{f}(\boldsymbol{x}) - \boldsymbol{u}(\boldsymbol{x}) \cdot \boldsymbol{K}(\boldsymbol{R}) \cdot \boldsymbol{n}(\boldsymbol{x})]\, \mathrm{d}S_x, \tag{C 1}$$

where $\boldsymbol{R} \equiv \boldsymbol{x} - \boldsymbol{x}_0$ and $\boldsymbol{J}$ and $\boldsymbol{K}$ are the velocity and stress tensors generated by a point force, given in two dimensions as

$$\boldsymbol{J} = (1/4\pi\lambda\mu)(-\boldsymbol{I} \log R + \boldsymbol{R}\boldsymbol{R}/R^2), \qquad \boldsymbol{K} = -(1/\pi)\boldsymbol{R}\boldsymbol{R}\boldsymbol{R}/R^4, \qquad R = |\boldsymbol{R}|. \tag{C 2}$$

The function $\chi(\boldsymbol{x}_0)$ has the value 1 if $\boldsymbol{x}_0$ lies strictly inside the fluid, zero if it lies outside and $\frac{1}{2}$ if $\boldsymbol{x}_0$ lies on the surface ∂S. The discontinuity arises from the term involving $\boldsymbol{K}$; since $\boldsymbol{K}$ is singular like $1/R$, the integral must be interpreted in a Cauchy-principal-value sense.

In two dimensions the formulation (C 1) presents potential difficulties for computation, especially in unbounded domains, because of the logarithmic growth of $\boldsymbol{J}$ as $R \to \infty$. We therefore develop an alternative formulation ((C 8) below) in which the traction $\boldsymbol{f}$ is written as a boundary integral of the velocity $\boldsymbol{u}$, for which the far field decays more rapidly. Taking $\boldsymbol{x}_0$ either inside or outside S, but not on the boundary ∂S, an expression for the pressure may be obtained from the Stokes equations, $\nabla p = \lambda\mu\, \nabla^2 \boldsymbol{u}$. Equation (C 1) gives

$$\chi(\boldsymbol{x}_0)\, p(\boldsymbol{x}_0) = \int_{\partial S} [\boldsymbol{L}(\boldsymbol{R}) \cdot \boldsymbol{f}(\boldsymbol{x}) + \boldsymbol{u}(\boldsymbol{x}) \cdot \boldsymbol{M}(\boldsymbol{R}) \cdot \boldsymbol{n}(\boldsymbol{x})]\, \mathrm{d}S_x, \tag{C 3}$$

where the tensors $\boldsymbol{L}$ and $\boldsymbol{M}$ are defined by

$$\boldsymbol{L} = -\boldsymbol{R}/2\pi R^2, \qquad \boldsymbol{M} = (\lambda\mu/\pi)(\boldsymbol{I}/R^2 - 2\boldsymbol{R}\boldsymbol{R}/R^4). \tag{C 4}$$

Since $\boldsymbol{\sigma} = -p\,\boldsymbol{I} + \lambda\mu(\nabla\boldsymbol{u} + \nabla\boldsymbol{u}^T)$ we can now write the stress in integral form:

$$\chi(\boldsymbol{x}_0)\, \boldsymbol{\sigma}(\boldsymbol{x}_0) \;=\; \int_{\partial S} [\boldsymbol{K}(\boldsymbol{R}) \cdot \boldsymbol{f}(\boldsymbol{x}) - \boldsymbol{u}(\boldsymbol{x}) \cdot \boldsymbol{N}(\boldsymbol{R}) \cdot \boldsymbol{n}(\boldsymbol{x})]\, \mathrm{d}S_x, \tag{C 5}$$

where

$$N_{ijkl} = \frac{\lambda\mu}{\pi}\left(\delta_{jk}\delta_{il}\frac{1}{R^2} + \delta_{ij}\frac{R_k R_l}{R^4} + \delta_{ik}\frac{R_j R_l}{R^4} + \delta_{jl}\frac{R_i R_k}{R^4} + \delta_{kl}\frac{R_i R_j}{R^4} - 8\frac{R_i R_j R_k R_l}{R^6}\right). \tag{C 6}$$

It is straightforward to check that $\nabla \cdot \boldsymbol{N} = 0$. Therefore we may replace $\boldsymbol{u}(\boldsymbol{x})$ by $\boldsymbol{u}(\boldsymbol{x}) - \boldsymbol{u}(\boldsymbol{x}_0)$ in equation (C 5), so that for any fixed vector $\boldsymbol{n}_0$

$$\chi(\boldsymbol{x}_0)\; \boldsymbol{\sigma}(\boldsymbol{x}_0) \cdot \boldsymbol{n}_0 \;=\; \int_{\partial S} [\boldsymbol{n}_0 \cdot \boldsymbol{K}(\boldsymbol{R}) \cdot \boldsymbol{f}(\boldsymbol{x}) - (\boldsymbol{u}(\boldsymbol{x}) - \boldsymbol{u}(\boldsymbol{x}_0)) \cdot \boldsymbol{N}(\boldsymbol{R}) \mathbf{:} \boldsymbol{n}(\boldsymbol{x})\boldsymbol{n}_0]\, \mathrm{d}S_x. \tag{C 7}$$

We now take the limit as $\boldsymbol{x}_0$ approaches the surface from either inside or outside S, noting the discontinuity in the integral involving $\boldsymbol{K}$ described above. We then regard $\boldsymbol{n}_0$ as the normal at $\boldsymbol{x}_0$, and

$$\tfrac{1}{2}\, \boldsymbol{f}(\boldsymbol{x}_0) = \fint_{\partial S} [\boldsymbol{n}(\boldsymbol{x}_0) \cdot \boldsymbol{K}(\boldsymbol{R}) \cdot \boldsymbol{f}(\boldsymbol{x}) - (\boldsymbol{u}(\boldsymbol{x}) - \boldsymbol{u}(\boldsymbol{x}_0)) \cdot \boldsymbol{N}(\boldsymbol{R}) : \boldsymbol{n}(\boldsymbol{x})\boldsymbol{n}(\boldsymbol{x}_0)]\, \mathrm{d}S_x. \tag{C 8}$$

This provides the integral expression for the surface traction in terms of the fluid velocity $\boldsymbol{u}(\boldsymbol{x}_0)$ on the boundary. Of course the problem posed can have a solution

only if the total force and couple acting on ∂S and the total mass flux through ∂S are all zero.

In the special case of a flow in the half-plane $Y \geqslant 0$ generated by tractions acting on the boundary $Y = 0$, symmetry implies that a purely tangential traction $f_t(x) = \boldsymbol{e}_x \cdot \boldsymbol{f}$ generates a purely tangential velocity $u_t(x) = \boldsymbol{e}_x \cdot \boldsymbol{u}$ on the boundary (and a purely normal traction generates a purely normal velocity on the boundary, see for example Jansons & Lister 1988). For a half-plane we have

$$\boldsymbol{n}(\boldsymbol{x}_0) \cdot \boldsymbol{K} = -(1/\pi R^4)\ \boldsymbol{n}(\boldsymbol{x}_0) \cdot \boldsymbol{R}\boldsymbol{R}\boldsymbol{R} = \boldsymbol{0}, \tag{C 9}$$

since $\boldsymbol{n} \cdot \boldsymbol{R} = \boldsymbol{0}$, and therefore for a purely tangential flow (C 8) reduces to

$$f_t(x_0) = -\frac{2\lambda\mu}{\pi} \int_{-\infty}^{\infty} \frac{u_t(x) - u_t(x_0)}{(x - x_0)^2}\, \mathrm{d}x. \tag{C 10}$$

Equation (C 10) can be derived directly for a half-plane by using (C 1) to write u_t in terms of f_t, then inverting using a Hilbert transform (Jacqmin 2002). The result (C 8) is more general, having applications to flows in other two-dimensional geometries.

REFERENCES

Bretherton, F. P. 1961 The motion of long bubbles in tubes. *J . Fluid Mech.*, **10**, 166–188.

Cachile, M., Chertcoff, R., Calvo, A., Rosen, M., Hulin, J. P. & Cazabat, A. M. 1996 Residual film dynamics in glass capillaries. *J. Colloid Interface Sci.* **182**, 483–491.

Carroll, B. J. & Lucassen, J. 1973 Capillarity-controlled entrainment of liquid by a thin cylindrical filament. *Chem. Engng Sci.* **28**, 23–30.

Chen, J. D. 1986 Measuring the film thickness surrounding a bubble inside a capillary. *J. Colloid Interface Sci.* **109**, 341–349.

Davis, R. H., Schonberg, J. A. & Rallison, J. M. 1989 The lubrication force between two viscous drops. *Phys. Fluids* A **1**, 93–106.

Fairbrother, F. & Stubbs, A. E. 1935 Studies in electroendosmosis. Part IV. The bubble-type method of measurement. *J. Chem. Soc.* **1**, 527–540.

Ghadiali, S. N. & Gaver, D. P. III 2003 The influence of non-equilibrium surfactant dynamics on the flow of a semi-infinite bubble in a rigid cylindrical capillary tube. *J. Fluid Mech.* **478**, 165–196.

Goldsmith, H. L. & Mason, S. G. 1963 The flow of suspensions through tubes. II. Single large bubbles. *J Colloid Sci.* **18**, 237–261.

Hodges, S. R. 2003 Hydrodynamics of fluid drops and cells near a wall. PhD Thesis, University of Cambridge.

Jacqmin, D. 2002 Very, very fast wetting. *J. Fluid Mech.* **455**, 347–358.

Jansons, K. M. & Lister, J. R. 1988 The general solution of Stokes flow in a half-space as an integral of the velocity on the boundary. *Phys. Fluids* **31**, 1321–1323.

Martinez, M. J. & Udell, K. S. 1990 Axisymmetric creeping motion of drops through circular tubes. *J. Fluid Mech.* **210**, 565–591.

Ou Ramdane, O. & Quéré, D. 1997 Thickening factor in Marangoni coating. *Langmuir* **13**, 2911–2916.

Park, C. W. 1991 Effects of insoluble surfactants on dip coating. *J. Colloid Interface Sci.* **146**, 382–394.

Park, C. W & Homsy, G. M. 1984 Two-phase development in Hele-Shaw cells: theory. *J. Fluid Mech.* **237**, 291–308.

Pozrikidis, C. 1992 *Boundary Integral and Singularity Methods for Linearized Viscous Flow*. Cambridge University Press.

Quéré, D. 1999 Fluid coating on a fiber. *Annu. Rev. Fluid Mech.* **31**, 347–384.

Quéré, D., De Ryck, A. & Ou Ramdane, O. 1997 Liquid coating from a surfactant solution. *Europhys. Lett.* **37**, 305–310.

Ratulowski, J. & Chang, H.-C. 1990 Marangoni effects of trace impurities on the motion of long gas bubbles in capillaries. *J. Fluid Mech.* **210**, 303–328.

Schwartz, L. W., Princen, H. M. & Kiss, A. D. 1986 On the motion of bubbles in capillary tubes. *J. Fluid Mech.* **172**, 259–275.

Shen, A. Q., Gleason, B., McKinley, G. H. & Stone, H. A. 2002 Fiber coating with surfactant solutions. *Phys. Fluids* **14**, 4055–4068.

Stebe, K. J., Lin, S. Y. & Maldarelli, C. 1991 Remobilizing surfactant retarded fluid particle interfaces. 1. Stress-free conditions at the interfaces of micellar solutions of surfactants with fast sorption kinetics. *Phys. Fluids* A **3**, 3–20.

Taylor, G. I. 1961 Deposition of a viscous fluid on the wall of a tube. *J. Fluid Mech.* **10**, 161–165.

Teletzke, G. F., Davis, H. T. & Scriven, L. E. 1988 Wetting hydrodynamics. *Revue Phys. Appl.* **23**, 989–1007.

Westborg, H. & Hassager, O. 1989 Creeping motion of long bubbles and drops in capillary tubes. *J. Colloid Interface Sci.* **133** 135–147.